

Bifurcation properties of nematic liquid crystals exposed to an electric field: Switchability, bistability, and multistability

L. J. Cummings, C. Cai, and L. Kondic

*Department of Mathematical Sciences and Center for Applied Mathematics and Statistics,
New Jersey Institute of Technology, Newark, New Jersey 07102, USA*

(Received 27 February 2013; published 30 July 2013)

Bistable liquid crystal displays (LCDs) offer the potential for considerable power savings compared with conventional (monostable) LCDs. The existence of two (or more) stable field-free states that are optically distinct means that contrast can be maintained in a display without an externally applied electric field. An applied field is required only to switch the device from one state to the other, as needed. In this paper we examine the basic physical principles involved in generating multiple stable states and the switching between these states. We consider a two-dimensional geometry in which variable surface anchoring conditions are used to control the steady-state solutions and explore how different anchoring conditions can influence the number and type of solutions and whether or not switching is possible between the states. We find a wide range of possible behaviors, including bistability, tristability, and tetrastability, and investigate how the solution landscape changes as the boundary conditions are tuned.

DOI: [10.1103/PhysRevE.88.012509](https://doi.org/10.1103/PhysRevE.88.012509)

PACS number(s): 42.70.Df, 61.30.Dk, 61.30.Gd, 61.30.Hn

I. INTRODUCTION

In e-ink display technology [1], spherical microcapsules are dispersed in a clear carrier fluid. Each microcapsule contains positively charged white particles and negatively charged black ones, which segregate in a dc electric field. If the electric field direction is reversed, so is the segregation of white and black particles in the microcapsule. Hence display contrast can be controlled by applying fields of appropriate polarities in different portions of the screen (pixels). Once the field is removed, the particles maintain their segregation within the microcapsule, so a field is required only to change the state of the display. Thus e-ink is a bistable technology and uses very little power, giving excellent battery lifetimes.

Most e-readers in current use rely on e-ink technology, but most portable phones, netbooks, and music players use conventional liquid crystal display (LCD) technology, which has better optical properties, but higher power consumption because it requires continuous application of an electric field. At the simplest level, an LCD pixel comprises a thin layer of nematic liquid crystal (NLC) sandwiched between two glass plates and placed between crossed polarizers. The NLC is birefringent: Depending on its internal molecular orientation, it can rotate the plane of polarized light. The molecular orientation can be controlled by boundary effects (so-called surface anchoring; depending on how a surface is prepared, the NLC molecules have a preferred orientation there) and by application of an electric field across the layer (its typically rodlike molecules align in an applied field). With the molecules aligned, the polarized light that passed through the first polarizer is not rotated as it passes through the NLC layer and is blocked by the second, crossed, polarizer. With no applied field, however, the molecular orientation within the layer is different (dictated solely by anchoring now, rather than the electric field); the polarized light is rotated as it passes through the NLC layer and can pass through the second crossed polarizer. These two states are therefore optically distinct when light is passed through (the first will be dark, the second bright)

and form the basis of an LCD. However, since the electric field must be on to maintain the contrast between neighboring pixels, such displays are energetically expensive.

One possible way to reduce the power consumption of an LCD device is to design it so that it is bistable, with two stable states for the molecular orientation in the absence of an applied electric field. Provided these stable states are optically distinct and may be switched from one to the other by *transient* application of an electric field, power consumption could rival that of e-ink technology, yet with superior optical properties. With no applied field the only way to control the molecular orientation within the device is by surface anchoring effects; hence to achieve bistability, control of surface anchoring is key. If anchoring conditions are chosen appropriately it is found that two (or more) steady states exist for the molecular orientation and that one can switch reversibly between the two states by applying an electric field across the bounding plates for a few milliseconds (see [2] and Sec. IV in the present paper).

In this paper we investigate theoretically a two-dimensional (2D) bistable LCD configuration that generalizes an earlier 1D model [2]. The 1D model considered a simple nematic sandwich between parallel bounding plates and relied on the premise that the bounding surfaces can be prepared so as to control the preferred molecular orientation of the nematic molecules (the anchoring angle) and the associated anchoring strengths, both being constant on each boundary. Here we consider a scenario in which anchoring properties (specifically, the anchoring angles) vary periodically along the bounding surfaces. This may be thought of as either a true variation in anchoring angle, due, e.g., to chemical gradients along the flat bounding surfaces or perhaps more realistically as an approximation to the anchoring variation induced by a periodically varying surface topography [as in, e.g., the Zenithal Bistable Device (ZBD) [3]]. We can view this problem as a perturbation to the associated 1D problem: The anchoring angles are of the form $\alpha = \alpha^{(0)} + \delta \cos(2\pi x^*/L^*)$, where $\alpha^{(0)}$ is the constant anchoring angle in the 1D problem, x^* is the coordinate parallel to the bounding surfaces, L^* is the

wavelength of the anchoring variation, and δ is the amplitude, which will play the role of a bifurcation parameter.

The paper is laid out as follows. In Sec. II we introduce the key dependent variables and outline the basic mathematical model in Secs. II A and II B. Section II C recaps the results of bistability and switching for the 1D model, presenting the full range of parameter space within which two-way switching is found. Section IV describes briefly the numerical approach taken and presents our key results. Finally in Sec. V we draw our conclusions.

II. MATHEMATICAL MODEL

The basic setup is a layer of NLC, sandwiched between parallel bounding surfaces at $z^* = 0$ and $z^* = h^*$. Star superscripts will be used throughout to denote dimensional quantities and will be dropped when we nondimensionalize. The molecules of the NLC are rodlike, which imparts anisotropy. The molecules tend to align locally, which is modeled by associating an elastic energy with any deviations from uniform alignment (Sec. II A). The local average molecular orientation is described by a director field \mathbf{n} , a unit vector that, in our 2D model, is confined to the (x^*, z^*) plane (see Fig. 1). It may therefore be expressed in terms of a single angle $\theta(x^*, z^*, t^*)$,

$$\mathbf{n} = (\sin \theta, 0, \cos \theta), \quad (1)$$

where t^* is time. We further assume that the electric field, when applied, is uniform throughout the NLC layer: $\mathbf{E}^* = E^*(t^*)(0, 0, 1)$. In reality the electric field and the NLC interact, so even if \mathbf{E}^* is uniform outside the layer, it will vary across the layer. A more careful treatment would take this into account; however, based on a preliminary investigation into variable field effects within a 1D device [4], we do not expect deviations from uniformity to be significant under normal operating conditions and we expect that the uniform field assumption is sufficient for the proof-of-principle investigation here. We recall that in any case an electric field is utilized only to switch the nematic configuration from one state to the other and therefore the detailed properties of the field are not so important.

Since we require bistability in the absence of an applied field, anchoring conditions at the bounding surfaces $z^* = 0, h^*$ are key. The anchoring pretilt angle (denoted by α in our model, the preferred value of θ at either interface) may be controlled by a variety of surface treatments; for example, mechanical or chemical treatments, nanopatterning, and surface irradiation have all been shown to produce certain desired anchoring angles [5–17] with a high degree of control. The anchoring strength A^* may also be controlled to some

extent [9, 11, 13, 14] by similar methods. As evidenced by these cited works, advances in the degree of control attainable are continually being made and, while not quite yet a reality, “bespoke surfaces” with desired anchoring properties are a real possibility for the near future. We shall therefore assume that surface anchoring angles and strengths are adjustable parameters, within a range of physically realistic values. We shall furthermore allow the anchoring angles to vary sinusoidally about some average value:

$$\alpha_i = \alpha_i^{(0)} + \delta_i \cos(2\pi x^*/L^* + \phi_i), \quad i = 0, 1, \quad (2)$$

$$\phi_0 = 0, \quad \phi_1 \in [0, \pi/2],$$

where $i = 0$ and 1 denote the lower and upper bounding surfaces, respectively, and $\phi_1 \neq 0$ allows for a phase difference between the variations on each surface. We expect that such periodic variation will approximate the situation in which the bounding surfaces themselves have periodically varying topography (possibly with a phase difference between upper and lower surfaces) as seen, for example, in the ZBD or post aligned bistable device (PABD) [3, 18]. We consider two cases for the amplitude parameters δ_0 and δ_1 : (i) They take the same value $\delta_1 = \delta_0 = \delta$ or (ii) $\delta_1 = 0$ and $\delta_0 = \delta$ (perturbation only on the lower boundary). Clearly, Eq. (2) is not the most general form of periodic anchoring variation that could be considered; nonetheless, we expect the results obtained as δ and L^* are varied to be representative of the more general case and in the interest of keeping the investigation manageable we restrict attention to this set of perturbations.

A. Energetics

The free energy of the liquid crystal layer, in the presence of an applied electric field and with specified anchoring conditions at each bounding surface, has several contributions. The bulk free energy density consists of elastic, dielectric, and flexoelectric contributions W_e^* , W_d^* , and W_f^* , respectively, and in our 2D model with the uniform field assumption these are given by

$$2W_e^* = K_1^*(\nabla^* \cdot \mathbf{n})^2 + K_3^*[(\nabla^* \times \mathbf{n}) \times \mathbf{n}]^2,$$

$$2W_d^* = -\varepsilon_0^*(\varepsilon_{\parallel} - \varepsilon_{\perp})(\mathbf{n} \cdot \mathbf{E}^*)^2,$$

$$W_f^* = -\mathbf{E}^* \cdot [e_1^*(\nabla^* \cdot \mathbf{n})\mathbf{n} + e_3^*(\nabla^* \times \mathbf{n}) \times \mathbf{n}],$$

where K_1^* and K_3^* are elastic constants, ε_0^* is the permittivity of free space, ε_{\parallel} and ε_{\perp} are the relative dielectric permittivities parallel and perpendicular to the long axis of the nematic molecules, and e_1^* and e_3^* are flexoelectric constants [19–21]. With the director field \mathbf{n} as given by Eq. (1) and the common simplifying assumption $K_1^* = K_3^* = K^*$, the total bulk free energy density $W^* = W_e^* + W_d^* + W_f^*$ simplifies. Introducing the nondimensional forms $W = K^*W^*/h^{*2}$ and $(x, z) = (x^*, z^*)/h^*$,

$$W = \frac{1}{2}(\theta_x^2 + \theta_z^2) - \mathcal{D} \cos^2 \theta + \frac{\mathcal{F}}{2}(\theta_z \sin 2\theta - \theta_x \cos 2\theta), \quad (3)$$

where

$$\mathcal{D} = \frac{h^{*2}E^{*2}\varepsilon_0^*(\varepsilon_{\parallel} - \varepsilon_{\perp})}{2K^*}, \quad \mathcal{F} = \frac{h^*E^*(e_1^* + e_3^*)}{K^*} \quad (4)$$

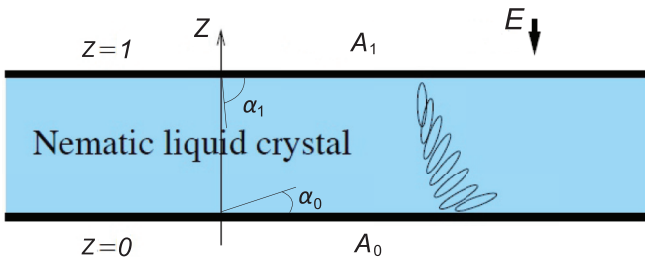


FIG. 1. (Color online) Sketch showing the setup and summarizing the key parameters in the dimensionless coordinates.

are dimensionless constants. With representative characteristic values $h^* \sim 2 \mu\text{m}$, $E^* \sim 1 \text{ V } \mu\text{m}^{-1}$, $e_1^* + e_3^* \sim 5 \times 10^{-11} \text{ C m}^{-1}$, $K^* \sim 1 \times 10^{-11} \text{ N}$, and $\varepsilon_{\parallel} - \varepsilon_{\perp} \sim 5$ [22–24], both \mathcal{D} and \mathcal{F} are $O(1)$. We emphasize that these values are *not* intended to be absolute; a fair degree of variation about these values is possible and indeed many different combinations of dimensional parameter values will lead to the same model in dimensionless form. Note that \mathcal{D} and \mathcal{F} are not independent; the ratio

$$\Upsilon = \frac{\mathcal{F}^2}{\mathcal{D}} = \frac{2(e_1^* + e_3^*)^2}{K^* \varepsilon_0^* (\varepsilon_{\parallel} - \varepsilon_{\perp})} \quad (5)$$

is a material parameter, independent of the geometry. We consider the most common case in which the dielectric anisotropy $\varepsilon_{\parallel} - \varepsilon_{\perp} > 0$ (molecules align parallel, rather than perpendicular, to an applied field) so that $\mathcal{D} > 0$ always. The parameter \mathcal{F} characterizing the dimensionless strength of the applied electric field will, however, change sign if the electric field direction is reversed. Since the representative parameter values listed above give $\Upsilon \approx 10$, we assign this value to Υ throughout our computations.

The surface anchoring is modeled by a Rapini-Papoular form [25]; if $g_{\{0,h^*\}}^* = (K^*/h^*)g_{\{0,1\}}$ are the surface energies per unit length at the boundaries $z^* = 0, h^*$, then

$$g_{0,1} = \frac{\mathcal{A}_{\{0,1\}}}{2} \sin^2(\theta - \alpha_{\{0,1\}}), \quad \mathcal{A}_{\{0,1\}} = \frac{h^* A_{\{0,h^*\}}^*}{K^*}, \quad (6)$$

where $A_{\{0,h^*\}}^*$ are the anchoring strengths at $z^* = 0, h^*$ and $\alpha_{\{0,1\}}$ are the preferred angles, given by Eq. (2): In dimensionless form,

$$\begin{aligned} \alpha_i &= \alpha_i^{(0)} + \delta_i \cos(2\pi x/L + \phi_i), \quad i = 0, 1, \\ \phi_0 &= 0, \quad \phi_1 \in [0, \pi/2], \end{aligned} \quad (7)$$

where the dimensionless perturbation wavelength $L = L^*/h^*$. As $\mathcal{A} \rightarrow \infty$ the anchoring becomes strong and the director angle is forced to take the value α . Figure 1 summarizes the setup and notation.

The total (dimensionless) free energy for the system is given by

$$\begin{aligned} J &= \int_0^1 \int_0^L W(\theta, \theta_z) dx dz \\ &+ \int_0^L g_0(x)|_{z=0} dx + \int_0^L g_1(x)|_{z=1} dx \end{aligned}$$

and equilibrium solutions are those functions $\theta(x, z)$ that minimize J . The standard calculus of variations approach, with $\theta(x, z) \mapsto \theta(x, z) + \epsilon \eta(x, z)$ ($0 < \epsilon \ll 1$) leads to $J \mapsto J[\theta + \epsilon \eta] = J_0 + \epsilon J_1 + \epsilon^2 J_2 + O(\epsilon^3)$ and for θ to be a minimizer of J we require $J_1 = 0$ and $J_2 > 0$ for all admissible variations η (the condition on J_2 ensures we have a minimum, rather than a maximum, of the free energy). After Taylor expansion and integration by parts

$$\begin{aligned} J_1 &= \int_0^1 \int_0^L \eta [W_{\theta} - (W_{\theta_z})_z - (W_{\theta_x})_x] dx dz \\ &+ \int_0^L \eta (g_{0\theta} - W_{\theta_z})|_{z=0} dx + \int_0^L \eta (g_{1\theta} + W_{\theta_z})|_{z=1} dx \\ &- \int_0^1 \eta W_{\theta_x}|_{x=0} dz + \int_0^1 \eta W_{\theta_x}|_{x=L} dz. \end{aligned}$$

The condition that this vanishes for all admissible variations η leads to the usual Euler-Lagrange equation for θ , subject to boundary conditions on $z = 0, 1$:

$$W_{\theta} - (W_{\theta_x})_x - (W_{\theta_z})_z = 0, \quad (8)$$

$$(g_{0\theta} - W_{\theta_z})|_{z=0} = 0, \quad (g_{1\theta} + W_{\theta_z})|_{z=1} = 0. \quad (9)$$

The net contribution to J_1 coming from $x = 0, 1$ is easily seen to vanish for the form of W specified by Eq. (3) if periodic boundary conditions on θ are enforced (both θ and θ_x continuous). We note that the second variation J_2 may be easily calculated if required to check stability. However, in practice we find all steady states by solving a diffusive equation arising from a gradient flow model (below), which guarantees that only stable steady states are found.

B. Time-dependent energetics: Gradient flow

As discussed in Ref. [2] for the 1D case, if the system is not initially at equilibrium then it will evolve over time towards a steady state described by the above equations. An accurate description of these dynamics requires the full equations of nematodynamics [20,26], which couple flow to director reorientation. For our explorations of parameter space that follow, however, the full model is extremely computationally intensive and instead we follow several other authors (e.g., Kedney and Leslie [27] and Davidson and Mottram [24]) in assuming that the system evolves in the direction that minimizes its total free energy (a gradient flow). Both bulk and surface components will evolve in this way and this process leads to

$$\begin{aligned} \theta_t + W_{\theta} - (W_{\theta_x})_x - (W_{\theta_z})_z &= 0, \\ (\tilde{\nu} \theta_t + g_{0\theta} - W_{\theta_z})|_{z=0} &= 0, \quad (\tilde{\nu} \theta_t + g_{1\theta} + W_{\theta_z})|_{z=1} = 0, \end{aligned}$$

with the choice of dimensionless time set by

$$t = t^* \frac{K^*}{\tilde{\mu}^* h^{*2}}, \quad (10)$$

where $\tilde{\mu}^*$ is the dimensional rotational viscosity of the NLC molecules, typically around 0.1 N s m^{-2} . The parameter $\tilde{\nu}$ is a dimensionless surface viscosity parameter of size $O(1)$ or smaller [24]; in practice simulations are not very sensitive to the exact value chosen for $\tilde{\nu}$ [28] and we set it to unity throughout. With bulk and surface energy densities given by Eqs. (3) and (6), the system becomes

$$\theta_t = \theta_{xx} + \theta_{zz} - \mathcal{D} \sin 2\theta, \quad (11)$$

$$\tilde{\nu} \theta_t = \theta_z - \frac{\mathcal{A}_0}{2} \sin 2(\theta - \alpha_0) + \frac{\mathcal{F}}{2} \sin 2\theta \quad \text{on } z = 0, \quad (12)$$

$$-\tilde{\nu} \theta_t = \theta_z + \frac{\mathcal{A}_1}{2} \sin 2(\theta - \alpha_1) + \frac{\mathcal{F}}{2} \sin 2\theta \quad \text{on } z = 1, \quad (13)$$

with \mathcal{D} (dimensionless dielectric coefficient), \mathcal{F} (dimensionless field strength), $\mathcal{A}_{\{0,1\}}$ (dimensionless surface energy), and $\alpha_{\{0,1\}}$ (anchoring angles) given by Eqs. (4), (6), and (7). An initial condition $\theta(x, z, 0)$ closes the model. When θ is independent of time, Eqs. (11)–(13) are exactly the steady-state model, specified by Eqs. (8) and (9). We will investigate the multistability and switching properties of Eqs. (11)–(13) as the anchoring perturbation parameters δ, L, ϕ are varied.

Before doing so, we first summarize the results of [2] for the analogous 1D model.

C. Summary of results of the 1D model

In the investigation of the 1D model in which anchoring conditions (and hence solutions) are independent of x , it was found that at sufficiently weak anchoring strengths, bistability is possible, with two-way switching between the stable states, effected by transient application of a moderate electric field across the bounding plates. The switching protocol adopted when attempting to switch between the stable steady states is as follows: A uniform electric field is applied at a fixed strength (characterized by a fixed value of $|\mathcal{F}|$ with both field directions considered) for t_1 dimensionless time units and then decreased linearly to zero over a further $t_1/4$ dimensionless time units. For the subset of investigations relevant to the present paper, the field strength was fixed at $|\mathcal{F}| = 5$, while t_1 was fixed at 20 (corresponding to a total dimensional switching time of about 150 ms).

The 1D model was optimized in the parameter space defined by parameters that may be varied in experiments: anchoring strengths and anchoring angles at the two surfaces. The optimization was carried out according to several criteria, principally: (i) maximize the anchoring strengths allowing two-way switching (to maximize robustness) and (ii) maximize the optical contrast between the two stable states. If specific weights are assigned to each of the criteria, an optimal configuration can be found and examples of this optimization are given in Ref. [2]. The optimization in that paper was carried out in stages, the first stage being an optimization to maximize surface energies (i) and contrast (ii), for the case in which the anchoring angle $\alpha_1^{(0)}$ at the upper surface is related to that at the lower surface $\alpha_0^{(0)}$ by

$$\alpha_1^{(0)} = \alpha_0^{(0)} - \pi/2. \quad (14)$$

Following this stage the anchoring angle $\alpha_1^{(0)}$ is allowed to vary independently and then further desirable criteria are introduced into the optimization.

In the final optimal states achieved in the subsequent trials, the anchoring angle $\alpha_1^{(0)}$ is quite close to $\alpha_0^{(0)} - \pi/2$. Therefore, when using this 1D model as the basis for the 2D geometry considered in the present work, we enforce the restriction given by Eq. (14), giving a smaller parameter space to consider. We also use the same switching protocol outlined above when testing for switching between the stable states, applying a field of dimensionless strength $|\mathcal{F}| = 5$ for a fixed time interval before decreasing the field linearly to zero. With these restrictions, the entire region of $(\mathcal{A}_0, \mathcal{A}_1, \alpha_0^{(0)})$ space within which bistability with two-way switching is achieved in the 1D model may be mapped out with reasonable computational effort. Figure 2 shows this region. For triplets $(\mathcal{A}_0, \mathcal{A}_1, \alpha_0^{(0)})$ outside this region, no two-way switching is found in the 1D model. Note in particular the existence of definitive upper bounds on the anchoring strengths \mathcal{A}_0 and \mathcal{A}_1 , at which the two-way switching is obtained. We also note that, where switching is achieved, in either direction, the sign of the electric field is always the same: $\mathcal{F} = -5$.

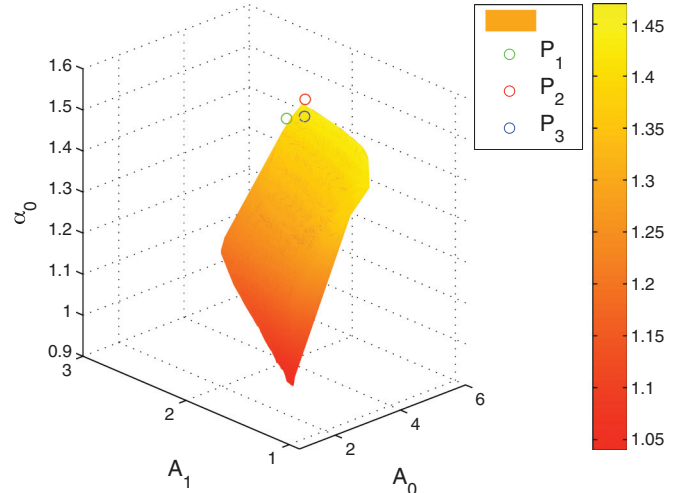


FIG. 2. (Color online) The 3D region of $(\mathcal{A}_0, \mathcal{A}_1, \alpha_0^{(0)})$ parameter space within which two-way switching is achieved for the 1D model, showing the particular points P_1 , P_2 , and P_3 used in our investigations of Sec. III. All points lying within the solid shaded region give two-way switching under the given switching protocol. The grayscale (color online) corresponds to the value of the anchoring angle at $z = 0$.

III. THE 2D MODEL INVESTIGATIONS

We investigate the effect of adding 2D boundary perturbations of the form (7) to the 1D model. This is motivated by several considerations: (i) It is likely that introducing spatial variation in the boundary will allow the region where two-way switching occurs to be extended, (ii) the 2D system is mathematically more complex and will likely lead to bifurcations to new steady states and the possible disappearance of old ones, and (iii) in any real device boundary variations are inevitable (even if due only to edge effects) and a 2D study will shed some light on the robustness of the 1D results.

We perturb the 1D model by replacing the constant anchoring angles $\alpha_0^{(0)}$ and $\alpha_1^{(0)}$ at the boundaries by sinusoidally varying angles given by Eq. (7) (with $\alpha_1^{(0)} = \alpha_0^{(0)} - \pi/2$). As noted, though such periodic perturbations are not the most general that could be considered, they do allow for a manageable parametric study to be carried out and we expect the results to be representative of the more general case. We may view such a perturbation either as due to surface treatment, which alters the surface chemistry and causes the anchoring angle to vary, or as an approximation to the changes in anchoring caused by topographical variation in the bounding surfaces (as in the ZBD or PABD devices [3,18]). One motivation for allowing such variations is to increase the size of the region where useful two-way switching is possible (relative to that for the 1D model) and a key consideration for robustness of a device to shocks is increasing the allowable anchoring strengths at which the device will work. Hence we first consider how this might be achieved.

We choose points $(\mathcal{A}_0, \mathcal{A}_1, \alpha_0^{(0)})$ in our parameter space that are *outside* the two-way switching region illustrated in Fig. 2, but close to its boundary. In particular, we increase the surface energies beyond the confines of the 1D switching region. For

such points two-way switching is not achievable within the 1D framework, but in two dimensions it may be possible. We choose three such points to investigate, all in the region of parameter space close to the highest allowable surface energies: points $P_1 = (5.41, 2.45, 1.40)$, $P_2 = (5.50, 2.30, 1.46)$, and $P_3 = (4.85, 2.10, 1.46)$. Other points (including some that are far from the 1D optimum) were investigated, but did not yield significantly different results from those for these three points.

For each chosen point we perturb the anchoring boundary conditions in several ways. (i) We perturb the anchoring only at the lower boundary. This involves setting $\delta_1 = 0$ in Eq. (7) and, with no loss of generality, $\phi_0 = 0$, leaving just two perturbation parameters δ and L . (ii) We perturb the anchoring at both boundaries, with the same amplitude $\delta_1 = \delta_0 = \delta$ and with no phase difference between the boundaries $\phi_0 = 0$, leaving just two perturbation parameters δ and L . (iii) We perturb the anchoring at both boundaries, with the same amplitude $\delta_1 = \delta_0 = \delta$ and with a variable phase difference between the boundaries $\phi_0 = \phi \in [0, \pi/2]$, but fixing the domain length L . This again leaves just two perturbation parameters δ and ϕ .

We describe the outcome of these investigations below. In all cases we use numerical continuation to generate our basic stable states. We start from the 1D problem, where the two stable steady states, which we label \mathbf{n}_1 and \mathbf{n}_2 , are known analytically [2]. We apply a small perturbation $\delta = 0.1$, using each 1D steady state as an initial condition in Eqs. (11)–(13) (at zero field, $\mathcal{D} = \mathcal{F} = 0$). We solve these equations using a standard alternating direction implicit scheme and look for steady-state solutions, which are in practice found by evolving Eqs. (11)–(13) until the results do not change further [typically it is enough to simulate until $t = 30$ (dimensionless time units) to ensure that true steady-state solutions are found]. Then we use these newly found steady-state solutions as initial conditions for the more strongly perturbed case, with $\delta = 0.2$ and so on. If at any stage a new steady state appears, backward

continuation in δ is used to locate its first appearance. We then subject all solutions found to our switching protocol (apply a transient electric field, as for the 1D case described in Sec. II C above). It is possible that this produces new steady states. If this happens, these states are also tracked using continuation in δ , as described above.

To illustrate further the coexistence of the multiple steady states and the transitions between them, we also construct bifurcation diagrams in several cases, by plotting a norm of the (stable) steady states versus δ :

$$\text{norm}(\mathbf{n}) := \sqrt{\sum_{i,j=1}^{M,N} \left(\frac{\theta_{i,j}(\text{mod}\pi)^2}{MN} \right)}, \quad (15)$$

where $\theta_{i,j}$ is the discretization of the director angle θ at grid point (i, j) and M and N are the total number of mesh grid points in each direction. The different steady states have different norms, hence the solution branches are distinct when plotted in this way and bifurcations are evident. Since (as described above) all steady states are found by time evolving the dynamic system until no further change is seen, this method of constructing the bifurcation diagram can produce only the stable solution branches. No unstable steady solutions are found by our methods.

IV. RESULTS

We summarize below our results for each type of boundary perturbation and for each of the three chosen test points in parameter space. The system exhibits rich behavior, with as many as four distinct steady states found in certain parameter regimes. We label these four steady states \mathbf{n}_1 , \mathbf{n}_2 , \mathbf{n}_3 , and \mathbf{n}_4 . In accordance with our continuation methods, \mathbf{n}_1 and \mathbf{n}_2 are always the continuations of the 1D steady states found in the unperturbed problem (consistent with the results of [2]), while \mathbf{n}_3 and \mathbf{n}_4 are new states that only exist with perturbed anchoring.

○ $\{\mathbf{n}_1, \mathbf{n}_2\}$ $\mathbf{n}_1 \rightarrow \mathbf{n}_2$	▽ $\{\mathbf{n}_1, \mathbf{n}_2, \mathbf{n}_3\}$ $\mathbf{n}_1 \rightarrow \mathbf{n}_3$	★ $\{\mathbf{n}_1, \mathbf{n}_2, \mathbf{n}_4\}$ $\mathbf{n}_1 \rightarrow \mathbf{n}_4, \mathbf{n}_4 \rightarrow \mathbf{n}_2$
○ $\{\mathbf{n}_1, \mathbf{n}_2, \mathbf{n}_3\}$ $\mathbf{n}_2 \rightarrow \mathbf{n}_1, \mathbf{n}_3 \rightarrow \mathbf{n}_2$	◁ $\{\mathbf{n}_1, \mathbf{n}_2, \mathbf{n}_3, \mathbf{n}_4\}$ $\mathbf{n}_1 \rightarrow \mathbf{n}_4, \mathbf{n}_3 \rightarrow \mathbf{n}_2$	☆ $\{\mathbf{n}_1, \mathbf{n}_2, \mathbf{n}_3, \mathbf{n}_4\}$ $\mathbf{n}_1 \rightarrow \mathbf{n}_3, \mathbf{n}_2 \rightarrow \mathbf{n}_3$
○ $\{\mathbf{n}_1, \mathbf{n}_2\}$ $\mathbf{n}_2 \rightarrow \mathbf{n}_1$	◄ $\{\mathbf{n}_1, \mathbf{n}_2, \mathbf{n}_4\}$ $\mathbf{n}_1 \rightarrow \mathbf{n}_4$	□ $\{\mathbf{n}_1, \mathbf{n}_2, \mathbf{n}_3, \mathbf{n}_4\}$ $\mathbf{n}_1 \rightarrow \mathbf{n}_3, \mathbf{n}_2 \rightarrow \mathbf{n}_4$
+ $\{\mathbf{n}_1, \mathbf{n}_2, \mathbf{n}_3\}$ $\mathbf{n}_1 \rightarrow \mathbf{n}_2, \mathbf{n}_3 \rightarrow \mathbf{n}_2$	◄ $\{\mathbf{n}_1, \mathbf{n}_2, \mathbf{n}_4\}$ $\mathbf{n}_1 \rightarrow \mathbf{n}_2, \mathbf{n}_4 \rightarrow \mathbf{n}_2$	◻ $\{\mathbf{n}_1, \mathbf{n}_2, \mathbf{n}_3, \mathbf{n}_4\}$ $\mathbf{n}_3 \rightarrow \mathbf{n}_1, \mathbf{n}_2 \rightarrow \mathbf{n}_4$
+ $\{\mathbf{n}_1, \mathbf{n}_2\}$ $\mathbf{n}_1 \leftrightarrow \mathbf{n}_2$	▷ $\{\mathbf{n}_1, \mathbf{n}_2, \mathbf{n}_3, \mathbf{n}_4\}$ $\mathbf{n}_1 \rightarrow \mathbf{n}_4, \mathbf{n}_3 \rightarrow \mathbf{n}_2, \mathbf{n}_4 \rightarrow \mathbf{n}_2$	● $\{\mathbf{n}_1, \mathbf{n}_2, \mathbf{n}_3, \mathbf{n}_4\}$
+ $\{\mathbf{n}_1, \mathbf{n}_2, \mathbf{n}_3\}$ $\mathbf{n}_1 \rightarrow \mathbf{n}_2, \mathbf{n}_3 \rightarrow \mathbf{n}_1$	▷ $\{\mathbf{n}_1, \mathbf{n}_2, \mathbf{n}_4\}$ $\mathbf{n}_2 \rightarrow \mathbf{n}_4$	● $\{\mathbf{n}_1, \mathbf{n}_2, \mathbf{n}_3, \mathbf{n}_4\}$ $\mathbf{n}_1 \rightarrow \mathbf{n}_4, \mathbf{n}_2 \rightarrow \mathbf{n}_4, \mathbf{n}_3 \rightarrow \mathbf{n}_4$
× $\{\mathbf{n}_1, \mathbf{n}_2, \mathbf{n}_3\}$ $\mathbf{n}_1 \rightarrow \mathbf{n}_3, \mathbf{n}_2 \rightarrow \mathbf{n}_3$	▷ $\{\mathbf{n}_1, \mathbf{n}_2, \mathbf{n}_3, \mathbf{n}_4\}$ $\mathbf{n}_2 \rightarrow \mathbf{n}_4$	● $\{\mathbf{n}_1, \mathbf{n}_2, \mathbf{n}_3\}$ $\mathbf{n}_2 \rightarrow \mathbf{n}_1, \mathbf{n}_3 \rightarrow \mathbf{n}_1$
× $\{\mathbf{n}_1, \mathbf{n}_2, \mathbf{n}_3\}$ $\mathbf{n}_2 \leftrightarrow \mathbf{n}_3, \mathbf{n}_1 \rightarrow \mathbf{n}_3$	◇ $\{\mathbf{n}_3\}$	◆ $\{\mathbf{n}_1, \mathbf{n}_2, \mathbf{n}_3, \mathbf{n}_4\}$ $\mathbf{n}_1 \rightarrow \mathbf{n}_4, \mathbf{n}_2 \rightarrow \mathbf{n}_1, \mathbf{n}_3 \rightarrow \mathbf{n}_1$
× $\{\mathbf{n}_1, \mathbf{n}_2, \mathbf{n}_3\}$ $\mathbf{n}_2 \rightarrow \mathbf{n}_1$	◇ $\{\mathbf{n}_1, \mathbf{n}_2, \mathbf{n}_4\}$ $\mathbf{n}_2 \rightarrow \mathbf{n}_1$	◆ $\{\mathbf{n}_1, \mathbf{n}_2, \mathbf{n}_3, \mathbf{n}_4\}$ $\mathbf{n}_1 \rightarrow \mathbf{n}_3$
* $\{\mathbf{n}_1, \mathbf{n}_2, \mathbf{n}_3\}$ $\mathbf{n}_1 \rightarrow \mathbf{n}_3, \mathbf{n}_2 \rightarrow \mathbf{n}_1$	◇ $\{\mathbf{n}_1, \mathbf{n}_2, \mathbf{n}_3\}$	◆ $\{\mathbf{n}_3, \mathbf{n}_4\}$
* $\{\mathbf{n}_1, \mathbf{n}_2, \mathbf{n}_3\}$ $\mathbf{n}_1 \rightarrow \mathbf{n}_3, \mathbf{n}_3 \rightarrow \mathbf{n}_2, \mathbf{n}_2 \rightarrow \mathbf{n}_1$	☆ $\{\mathbf{n}_1, \mathbf{n}_2\}$	■ $\{\mathbf{n}_1, \mathbf{n}_2, \mathbf{n}_3, \mathbf{n}_4\}$ $\mathbf{n}_2 \rightarrow \mathbf{n}_3$
△ $\{\mathbf{n}_2, \mathbf{n}_3\}$ $\mathbf{n}_3 \rightarrow \mathbf{n}_2$	☆ $\{\mathbf{n}_1, \mathbf{n}_3\}$	■ $\{\mathbf{n}_1, \mathbf{n}_2, \mathbf{n}_3, \mathbf{n}_4\}$ $\mathbf{n}_1 \rightarrow \mathbf{n}_2, \mathbf{n}_3 \rightarrow \mathbf{n}_2, \mathbf{n}_4 \rightarrow \mathbf{n}_2$
▽ $\{\mathbf{n}_1, \mathbf{n}_2, \mathbf{n}_3, \mathbf{n}_4\}$ $\mathbf{n}_1 \rightarrow \mathbf{n}_3, \mathbf{n}_4 \rightarrow \mathbf{n}_2$	☆ $\{\mathbf{n}_3, \mathbf{n}_4\}$ $\mathbf{n}_3 \rightarrow \mathbf{n}_4$	▲ $\{\mathbf{n}_1, \mathbf{n}_2, \mathbf{n}_3, \mathbf{n}_4\}$ $\mathbf{n}_1 \rightarrow \mathbf{n}_2, \mathbf{n}_3 \rightarrow \mathbf{n}_2$
▽ $\{\mathbf{n}_1, \mathbf{n}_3\}$ $\mathbf{n}_1 \rightarrow \mathbf{n}_3$	☆ $\{\mathbf{n}_1, \mathbf{n}_2, \mathbf{n}_4\}$ $\mathbf{n}_1 \rightarrow \mathbf{n}_4, \mathbf{n}_2 \rightarrow \mathbf{n}_4$	▼ $\{\mathbf{n}_1, \mathbf{n}_2, \mathbf{n}_3, \mathbf{n}_4\}$ $\mathbf{n}_1 \rightarrow \mathbf{n}_4, \mathbf{n}_2 \rightarrow \mathbf{n}_3$

FIG. 3. (Color online) Explanation of symbols used in the switching results that follow below. The notation within curly brackets denotes which steady states exist at a given point in parameter space. The statement $\mathbf{n}_i \rightarrow \mathbf{n}_j$ denotes that switching occurs from state \mathbf{n}_i to \mathbf{n}_j and $\mathbf{n}_i \leftrightarrow \mathbf{n}_j$ denotes that two-way switching occurs between states \mathbf{n}_i and \mathbf{n}_j .

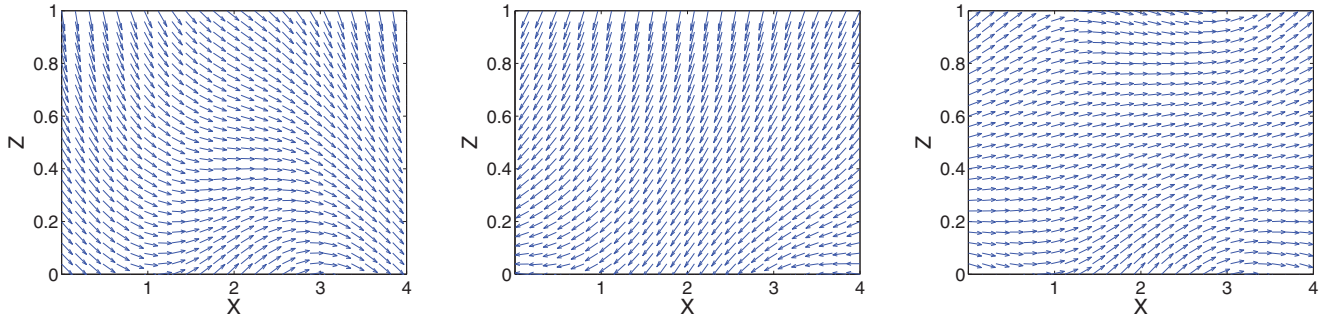


FIG. 4. (Color online) The three steady states (a) \mathbf{n}_1 , (b) \mathbf{n}_2 , and (c) \mathbf{n}_3 , corresponding to the point $(L, \delta) = (4, 0.7)$ in Fig. 5.

The results on switching are presented symbolically to denote the outcome at each point in parameter space, with reference to the global legend presented in Fig. 3. Each symbol in that legend records which steady states exist (listed within curly brackets) and what switching is found between those states (denoted by directional arrows as described in the caption). An example of three coexisting steady states is shown in Fig. 4.

We note that exploring the complete 3D parameter space considered would be computationally very demanding. The discussion that follows is limited to illustrating just some features of the results that may be expected.

A. Equal-amplitude perturbations to anchoring angles at both boundaries with zero phase difference

Here we consider the domain with anchoring angles α_0 and α_1 at lower and upper boundaries given by

$$\begin{aligned} \alpha_0 &= \alpha_0^{(0)} + \delta \cos(2\pi x/L), \\ \alpha_1 &= \alpha_0^{(0)} - \pi/2 + \delta \cos(2\pi x/L) \end{aligned} \tag{16}$$

as the perturbation amplitude δ and domain length L vary.

1. Point $P_1: (\mathcal{A}_0, \mathcal{A}_1, \alpha_0^{(0)}) = (5.41, 2.45, 1.40)$

Figure 5 shows the results of the switching investigation when the 1D case represented by point P_1 in $(\mathcal{A}_0, \mathcal{A}_1, \alpha_0^{(0)})$ space is perturbed at both boundaries, with no phase difference, as in Eq. (16). We see that for sufficiently small perturbation amplitude δ the continuations of the two 1D stable steady states exist and there is still no two-way switching between them. This is to be anticipated since the point P_1 lies outside the switching region for the 1D problem. As δ increases however, more complex behavior emerges.

For sufficiently small values of L , once δ passes a first threshold value, a window of two-way switching $\mathbf{n}_1 \leftrightarrow \mathbf{n}_2$ is observed. This is already a significant finding since it shows that two-way switching is possible in the 2D geometry even if it does not occur for the 1D case. This window disappears when δ passes a second threshold value. Both threshold values decrease as L increases. When δ is increased further still, a new steady state \mathbf{n}_3 is observed. As an illustration, Fig. 4 shows \mathbf{n}_1 , \mathbf{n}_2 , and \mathbf{n}_3 as vector plots in (x, z) space over a single wavelength for $(L, \delta) = (4, 0.7)$.

For small values of L , \mathbf{n}_3 appears to arise from a pitchfork bifurcation of \mathbf{n}_1 and \mathbf{n}_2 , as shown in Fig. 6. This figure shows a bifurcation diagram, constructed by plotting a norm of the

(stable) steady states versus δ [see Eq. (15)]. Figure 6 shows bifurcation diagrams for the cases $L = 0.5$ and 4: The case $L = 0.5$ clearly indicates the pitchfork bifurcation. For this value of L the stable steady state \mathbf{n}_3 never coexists with stable steady states \mathbf{n}_1 and \mathbf{n}_2 , but replaces them at large δ . As described in Sec. III, these bifurcation diagrams show only the stable solution branches; unstable steady solutions are not found by our methods.

Figure 5 shows that for larger values of L , $L \gtrsim 2$, the two-way switching between \mathbf{n}_1 and \mathbf{n}_2 is suppressed. The stable steady state \mathbf{n}_3 appears sooner, at smaller values of δ , and now coexists with \mathbf{n}_1 and \mathbf{n}_2 . For $L = 3$, although there is no two-way switching $\mathbf{n}_1 \leftrightarrow \mathbf{n}_2$, we do find two-way switching between \mathbf{n}_2 and \mathbf{n}_3 [for $\delta = 0.6, 0.7$ and presumably also in some surrounding neighborhood of (L, δ) space] and for $\delta = 0.5$ it is particularly interesting to observe *cyclic* switching involving all three steady states: We see the switching sequence $\mathbf{n}_1 \rightarrow \mathbf{n}_3 \rightarrow \mathbf{n}_2 \rightarrow \mathbf{n}_1$. We expect that this cyclic switching occurs in some small surrounding neighborhood of (L, δ) space.

For $L = 6$ (the largest value of L considered) the steady state \mathbf{n}_3 appears even for the smallest value of δ used, $\delta = 0.1$. More generally, though more steady states exist with (one would imagine) greater potential for switchability for larger L , no two-way switching is found for $L > 3$.

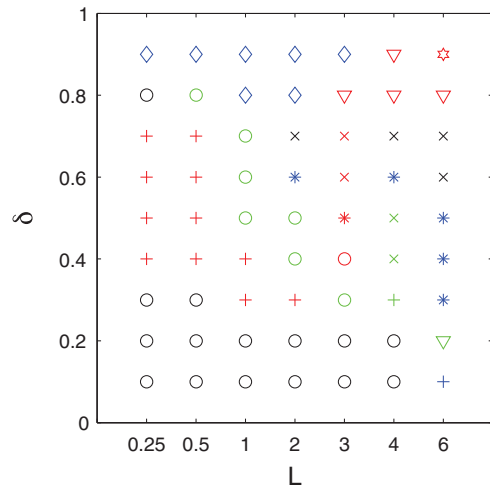


FIG. 5. (Color online) Switching results when perturbing the 1D case represented by point P_1 , $(\mathcal{A}_0, \mathcal{A}_1, \alpha_0^{(0)}) = (5.41, 2.45, 1.40)$, according to Eq. (16). Symbols are defined in the global legend of Fig. 3.

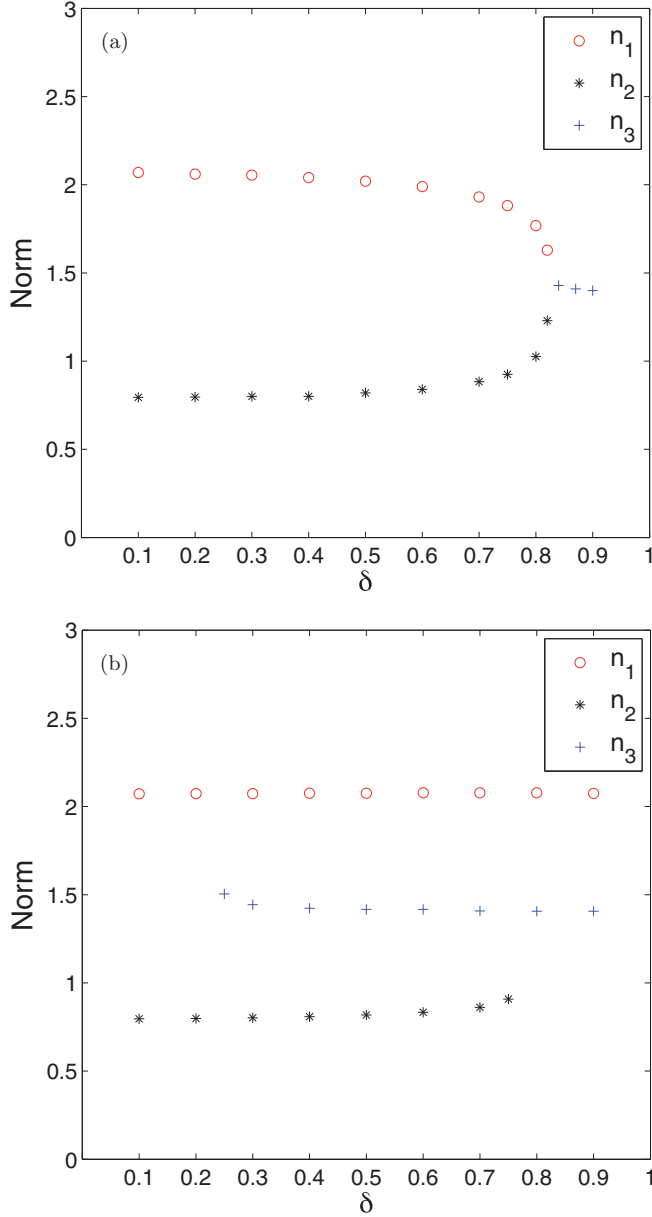


FIG. 6. (Color online) Bifurcation diagrams representing stable steady states obtained when perturbing the 1D case represented by point P_1 , $(\mathcal{A}_0, \mathcal{A}_1, \alpha_0^{(0)}) = (5.41, 2.45, 1.40)$, for the cases (a) $L = 0.5$ and (b) $L = 4$.

Another consequence of longer domains (larger L) is an increased degree of solution complexity, as is apparent from the bifurcation diagram shown in Fig. 6(b).

The steady state n_3 , once formed, appears rather robust under the conditions investigated here: Other than the switching noted above for $L = 3$ as well as $n_3 \rightarrow n_2$ switching at small δ for $L = 6$, no switching was found from this state to any other. Far more switching is found from the steady states n_1 and n_2 to other states.

2. Point P_2 : $(\mathcal{A}_0, \mathcal{A}_1, \alpha_0^{(0)}) = (5.50, 2.30, 1.46)$

Figure 7 shows results when the 1D case represented by point P_2 in $(\mathcal{A}_0, \mathcal{A}_1, \alpha^{(0)})$ is perturbed at both boundaries, with

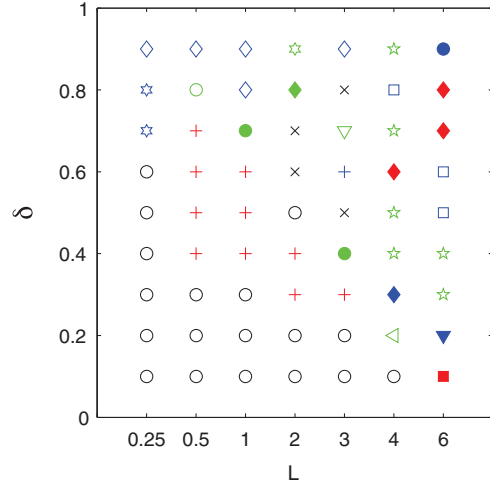


FIG. 7. (Color online) Switching results when perturbing the 1D case represented by point P_2 , $(\mathcal{A}_0, \mathcal{A}_1, \alpha_0^{(0)}) = (5.50, 2.30, 1.46)$, according to Eq. (16). Symbols are defined in the global legend of Fig. 3.

no phase difference, as in Eq. (16). For very short domains, no two-way switching is found, at any perturbation amplitude. Only the two steady states n_1 and n_2 exist until $\delta = 0.9$, when the third steady state n_3 appears. This state replaces both n_1 and n_2 ; see also the bifurcation plot in Fig. 8(a). As the length L is increased slightly (as with the point P_1) a window of two-way switching opens for a range of δ values. Again, at higher δ the third steady state n_3 appears and the δ value at which n_3 appears decreases as L increases. At $L = 2$ yet another steady state n_4 appears at large δ : At this L value as δ increases we have just two steady states for $0 \leq \delta \leq 0.5$, with two-way switching for $\delta = 0.3, 0.4$; for $\delta = 0.6, 0.7$ three steady states n_1, n_2 , and n_3 coexist; for $\delta = 0.8$ just n_3 exists; and for $\delta = 0.9$ the new steady state n_4 comes into existence, coexisting with n_3 . No further two-way switching is found however. For larger values $L > 3$, though the solution space becomes much richer and more complex, no two-way switching is found between any pair of stable states, even though for some parameter ranges all four steady states can coexist [see the bifurcation diagram for $L = 4$ in Fig. 8(b) where the four states coexist for a wide range of δ values]. The steady state n_4 appears to be particularly stable here since it does not switch to any other state.

The trend of two-way switching for smaller domains and of increased solution complexity for longer domains is as seen for the point P_1 described above. Increased complexity could be loosely explained based on the increased ability of the director orientation to find additional configurations; however, we do not have a good explanation for the lack of two-way switching for these large domains.

Examples of the four steady states that can coexist are shown in Fig. 9.

3. Point P_3 : $(\mathcal{A}_0, \mathcal{A}_1, \alpha_0^{(0)}) = (4.85, 2.10, 1.46)$

Figure 10 shows results when the 1D case represented by point P_3 in $(\mathcal{A}_0, \mathcal{A}_1, \alpha^{(0)})$ space is perturbed at both boundaries, with no phase difference, as in Eq. (16). This case differs from the previous two: The region of two-way switching has

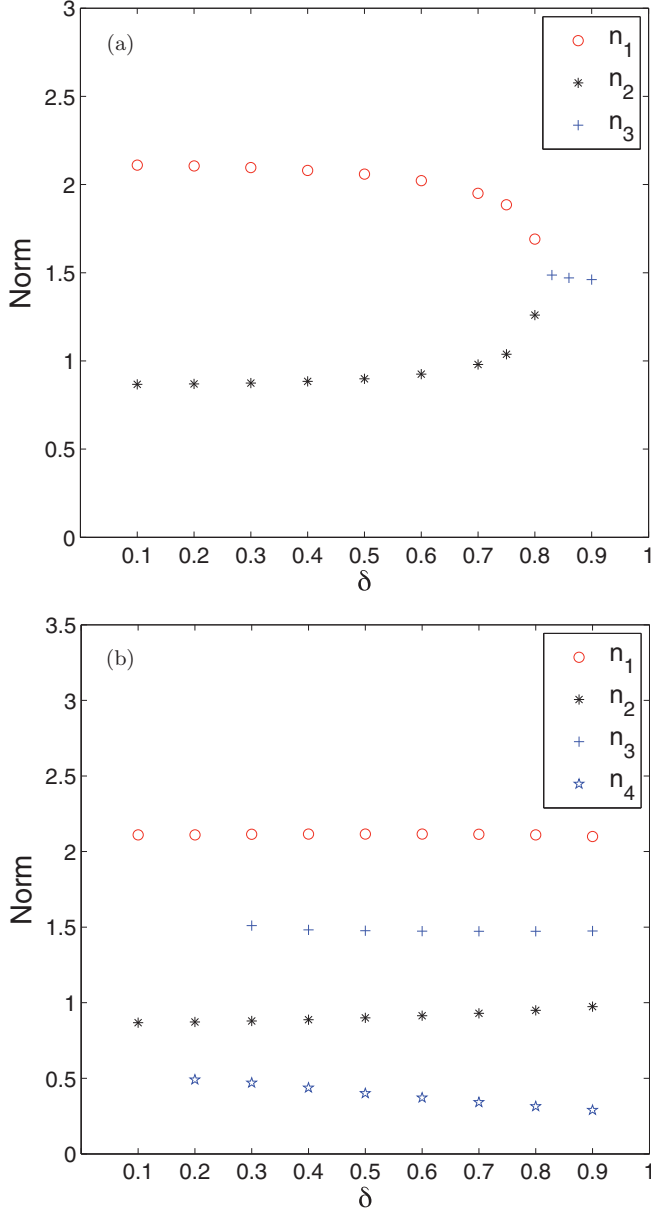


FIG. 8. (Color online) Bifurcation diagrams representing stable steady states obtained when perturbing the 1D case represented by point P_2 , $(\mathcal{A}_0, \mathcal{A}_1, \alpha_0^{(0)}) = (5.50, 2.30, 1.46)$, for the cases (a) $L = 0.5$ and (b) $L = 4$.

shrunk considerably, to some small neighborhood of the point $(L, \delta) = (1, 0.5)$. As with the two other points though, the solution space complexity increases markedly as L increases:

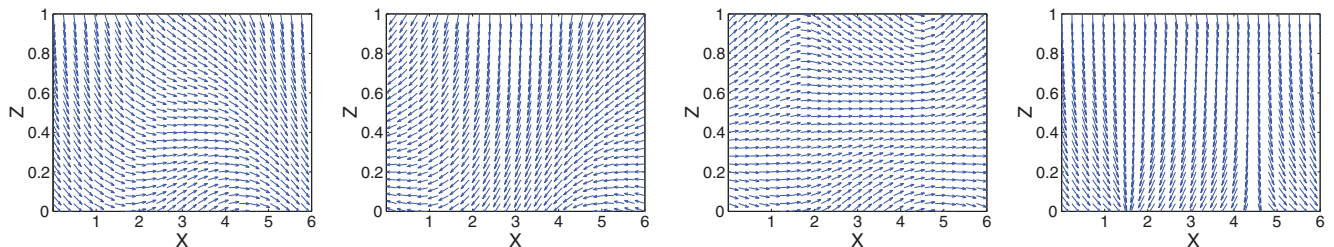


FIG. 9. (Color online) The four steady states (a) n_1 , (b) n_2 , (c) n_3 , and (d) n_4 , corresponding to the point $(L, \delta) = (6, 0.6)$ in Fig. 7.

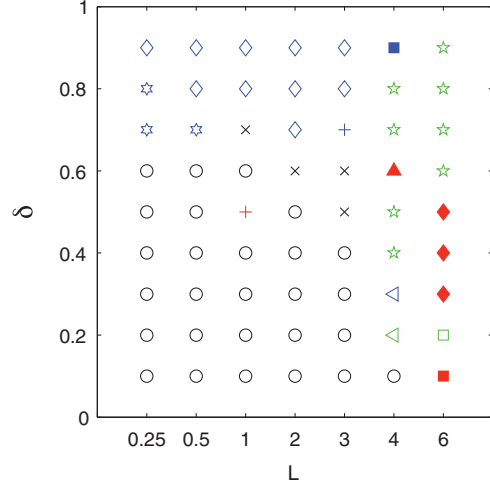


FIG. 10. (Color online) Switching results when perturbing the 1D case represented by point P_3 , $(\mathcal{A}_0, \mathcal{A}_1, \alpha_0^{(0)}) = (4.85, 2.10, 1.46)$, according to Eq. (16). Symbols are defined in the global legend of Fig. 3.

For $L \geq 1$ we find that three solutions can coexist ($n_1, n_2,$ and n_3), while for $L \geq 4$ we again find four solutions that can coexist for a wide range of δ values. This increase in solution complexity may again be illustrated by bifurcation diagrams as the bifurcation parameter δ is increased: Fig. 11 shows the bifurcation diagrams for $L = 0.5$ and 4. As usual, the shorter domain length leads to a simple pitchfork bifurcation.

B. Equal-amplitude perturbations to anchoring angles at both boundaries with phase difference

In this section we consider the case with anchoring angles α_0 and α_1 at lower and upper boundaries given by

$$\begin{aligned} \alpha_0 &= \alpha_0^{(0)} + \delta \cos(2\pi x/L + \phi), \\ \alpha_1 &= \alpha_0^{(0)} - \pi/2 + \delta \cos(2\pi x/L) \end{aligned} \quad (17)$$

as the perturbation amplitude δ and phase shift ϕ vary. For each point in parameter space considered, motivated by the underlying application (which requires two-way switching for utility), we fix the domain length L at the most promising value indicated by the results of Sec. IV A.

1. Point P_1 : $(\mathcal{A}_0, \mathcal{A}_1, \alpha_0^{(0)}) = (5.41, 2.45, 1.40)$

For this point, the (equal) best domain length in terms of achieving the largest window of two-way switching,

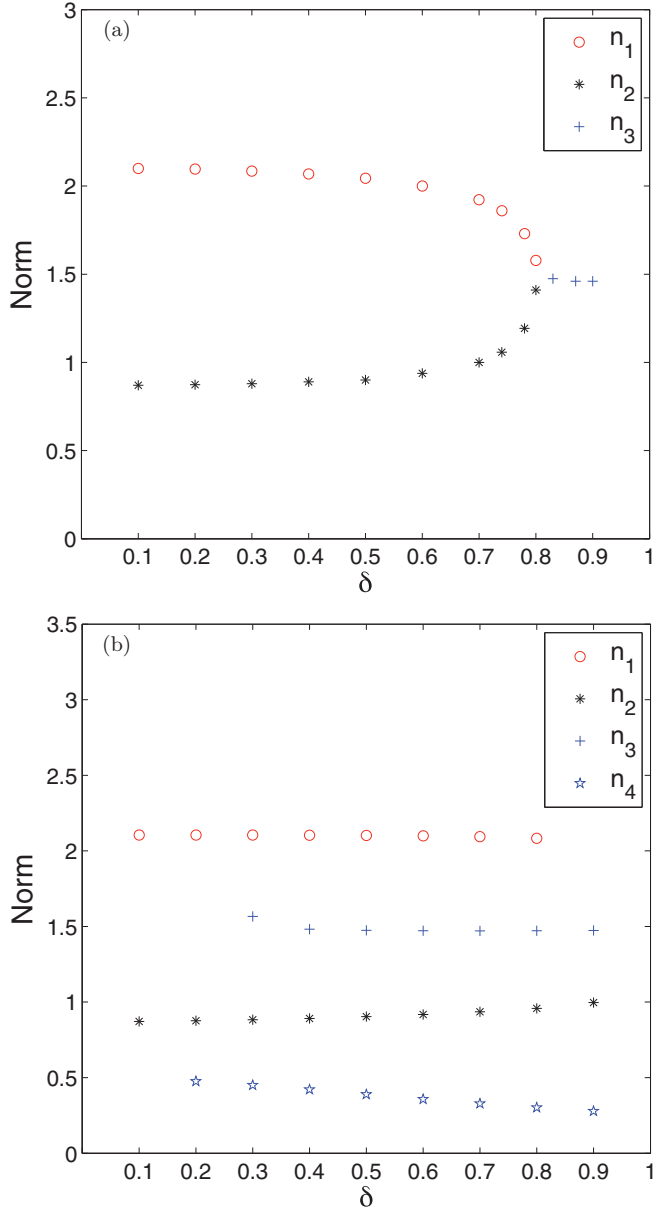


FIG. 11. (Color online) Bifurcation diagrams representing stable steady states obtained when perturbing the 1D case represented by point P_3 , $(\mathcal{A}_0, \mathcal{A}_1, \alpha_0^{(0)}) = (4.85, 2.10, 1.46)$, for the cases (a) $L = 0.5$ and (b) $L = 4$.

as indicated by the results of Sec. IV A, Fig. 5, is $L = 0.5$. We therefore consider the influence of introducing a phase difference ϕ into the anchoring variations on both boundaries, as indicated in Eq. (17) above, with L fixed at this value.

Figure 12 shows the results as the phase difference in boundary conditions [Eq. (17)] is increased from $\phi = 0$ to $\phi = \pi$. Note that for this and the subsequent points considered, the results for $\pi \leq \phi \leq 2\pi$ may be obtained by reflecting Fig. 12 about $\phi = \pi$. Curiously, the results are almost independent of the phase difference, a sizable window of two-way switching persisting for all values of ϕ tested. No pattern of increasing solution complexity emerges here: The third steady state n_3 is

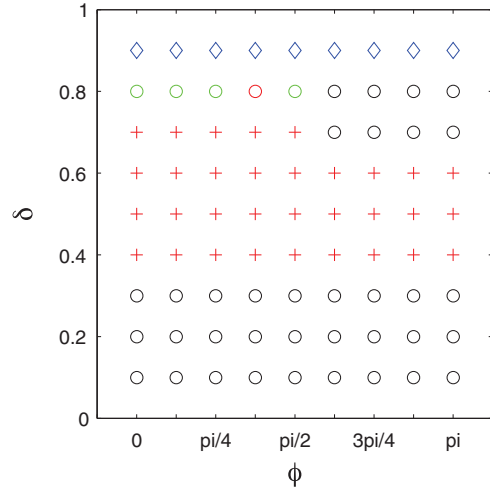


FIG. 12. (Color online) Switching results when perturbing the 1D case represented by point P_1 , $(\mathcal{A}_0, \mathcal{A}_1, \alpha_0^{(0)}) = (5.41, 2.45, 1.40)$, according to Eq. (17). The domain length is fixed at $L = 0.5$. Symbols are defined in the global legend of Fig. 3.

always observed only for large δ and no fourth steady state is found.

2. Point P_2 : $(\mathcal{A}_0, \mathcal{A}_1, \alpha_0^{(0)}) = (5.50, 2.30, 1.46)$

For this point, the best domain length in terms of achieving the largest window of two-way switching, as indicated by the results of Sec. IV A, Fig. 7, is again $L = 0.5$. Figure 13 shows the results as the phase difference in Eq. (17) is increased from $\phi = 0$ to $\phi = \pi$. In this case the window of two-way switching shrinks as ϕ is increased and eventually disappears. Otherwise, the behavior is similar to that observed for point P_1 above: There is no evidence of increasing solution complexity as ϕ is varied, n_3 is found only at large δ , and no fourth steady state is ever found.

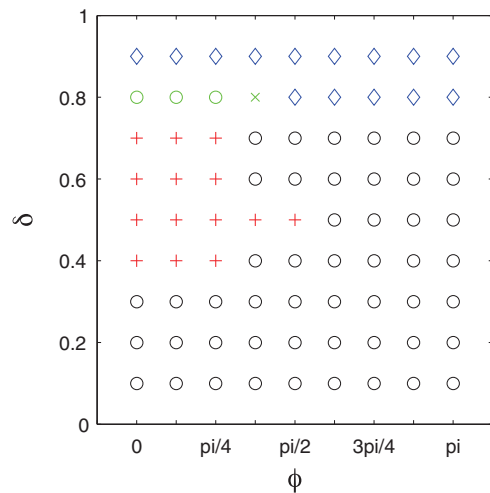


FIG. 13. (Color online) Switching results when perturbing the 1D case represented by point P_2 , $(\mathcal{A}_0, \mathcal{A}_1, \alpha_0^{(0)}) = (5.50, 2.30, 1.46)$, according to Eq. (17). The domain length is fixed at $L = 0.5$. Symbols are defined in the global legend of Fig. 3.

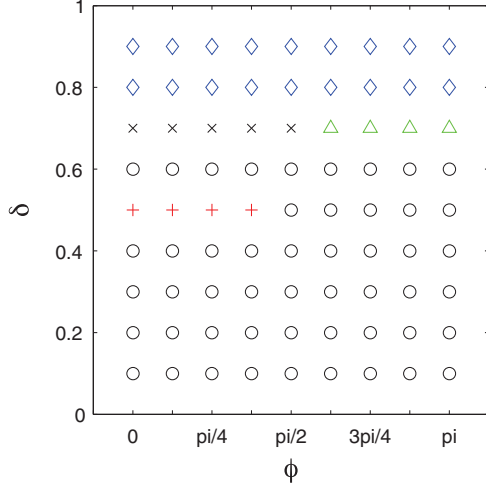


FIG. 14. (Color online) Switching results when perturbing the 1D case represented by point P_3 , $(\mathcal{A}_0, \mathcal{A}_1, \alpha_0^{(0)}) = (4.85, 2.10, 1.46)$, according to Eq. (17). The domain length is fixed at $L = 1$. Symbols are defined in the global legend of Fig. 3.

3. Point P_3 : $(\mathcal{A}_0, \mathcal{A}_1, \alpha_0^{(0)}) = (4.85, 2.10, 1.46)$

For this point, two-way switching was observed in the results of Sec. IV A only for the domain length $L = 1$ (see Fig. 10), hence we set $L = 1$ here.

Figure 14 shows the results as the phase difference in Eq. (17) is increased from $\phi = 0$ to $\phi = \pi$. As with point P_1 , little variation with ϕ is observed. The small window of two-way switching persists until $\phi = \pi/2$, after which it vanishes. The steady state n_3 appears at the same δ value for all phase shifts ϕ ($\delta = 0.7$), in coexistence with n_1 and n_2 for $0 \leq \phi \leq \pi/2$ and in coexistence with n_2 only for $\phi > \pi/2$ (so the bifurcation structure changes slightly as ϕ is increased).

To conclude, though we carried out only limited tests, it does not appear that introducing phase difference into the boundary conditions leads to increased two-way switching.

C. Perturbation to anchoring angle at one boundary only

In this section we investigate the effects of anchoring variations at one bounding surface only (we choose the lower surface). The anchoring angles imposed when solving Eqs. (11)–(13) are

$$\alpha_0 = \alpha_0^{(0)} + \delta \cos(2\pi x/L), \quad \alpha_1 = \alpha_0^{(0)} - \pi/2. \quad (18)$$

1. Point P_1 : $(\mathcal{A}_0, \mathcal{A}_1, \alpha_0^{(0)}) = (5.41, 2.45, 1.40)$

Figure 15 shows that, in line with our earlier results, increasing the domain length L is associated with increasing solution complexity, though the switching obtained is less complex than in Sec. IV A, where both boundaries are perturbed. No two-way switching is ever found, nor any switching cycles, therefore, in this instance at least, perturbing just the one boundary does not appear to be advantageous.

2. Point P_2 : $(\mathcal{A}_0, \mathcal{A}_1, \alpha_0^{(0)}) = (5.50, 2.30, 1.46)$

Figure 16 shows the results of a perturbation represented by Eq. (18) to the anchoring conditions on the lower boundary

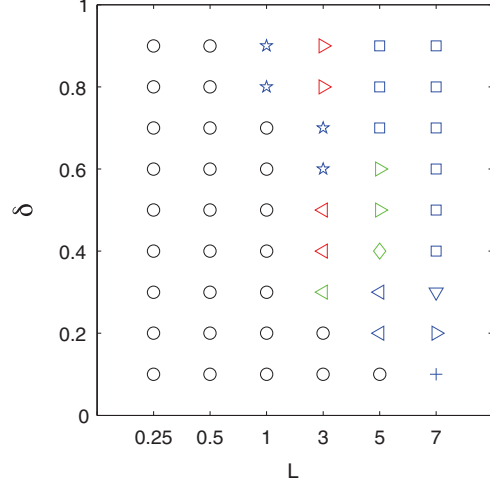


FIG. 15. (Color online) Switching results when perturbing the 1D case represented by point P_1 , $(\mathcal{A}_0, \mathcal{A}_1, \alpha_0^{(0)}) = (5.41, 2.45, 1.40)$, according to Eq. (18). The lower boundary only is perturbed and δ and L vary. Symbols are defined in the global legend of Fig. 3.

only, the unperturbed case being represented by point P_2 in the 1D problem. The same general observations as for point P_1 above hold: Again, increasing the domain length L is clearly associated with increasing solution complexity, but the behavior is overall less complex than in Sec. IV A, where both boundaries are perturbed. No two-way switching or switching cycles are found for any (L, δ) values tested, therefore, for P_2 this type of boundary perturbation also does not lead to desired two-way switching.

3. Point P_3 : $(\mathcal{A}_0, \mathcal{A}_1, \alpha_0^{(0)}) = (4.85, 2.10, 1.46)$

Figure 17 shows the results for point P_3 in the 1D problem. This case behaves similarly to points P_1 and P_2 above, with increasing L leading to increased complexity, but with no useful two-way or cyclic switching found.

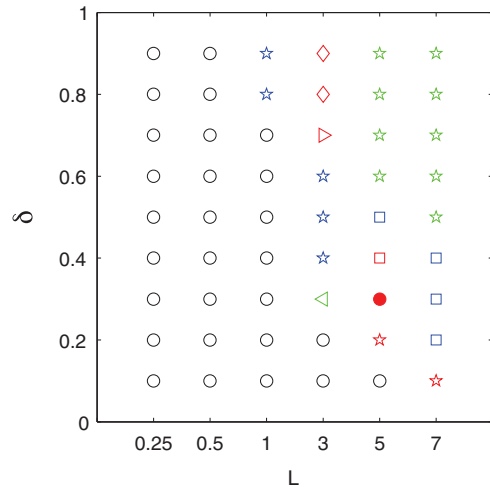


FIG. 16. (Color online) Switching results when perturbing the 1D case represented by point P_2 , $(\mathcal{A}_0, \mathcal{A}_1, \alpha_0^{(0)}) = (5.50, 2.30, 1.46)$, according to Eq. (18). The lower boundary only is perturbed and δ and L vary. Symbols are defined in the global legend of Fig. 3.

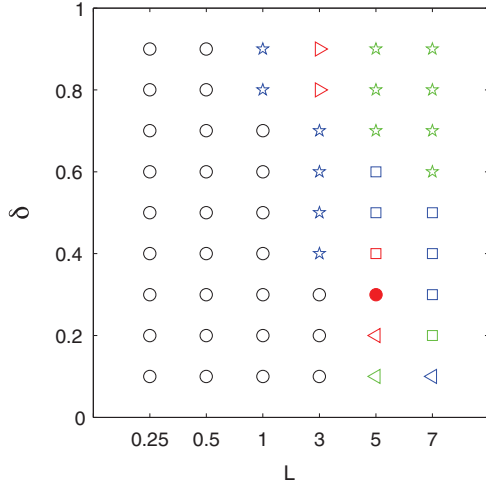


FIG. 17. (Color online) Switching results when perturbing the 1D case represented by point P_3 , $(\mathcal{A}_0, \mathcal{A}_1, \alpha_0^{(0)}) = (4.85, 2.10, 1.46)$, according to Eq. (18). The lower boundary only is perturbed and δ and L vary. Symbols are defined in the global legend of Fig. 3.

V. DISCUSSION AND CONCLUSIONS

We have taken a basic but promising 1D model for a bistable LCD device [2] and investigated how it behaves under a specific class of spatial perturbations to the anchoring boundary conditions (sinusoidal perturbations to the anchoring angles at the flat bounding surfaces). While more general periodic boundary perturbations could be considered, we restrict attention to those of the form (7) because they afford a manageable parameter space to study and we believe the results will be representative of the more general case. Such perturbations to the anchoring angles could be due to periodic chemical gradients imposed at the surfaces or may be thought of as approximating a device with periodic topographical variations. The study of such variations is important for two reasons: First, it may provide useful indications of how to tune boundaries to create a workable bistable device of this kind, which improves on the simpler 1D model proposed in Ref. [2]; and second, it affords insight into the robustness of the underlying 1D device to engineering imperfections.

Our results are presented for a few chosen sample points in the space of surface energies \mathcal{A}_0 and \mathcal{A}_1 at the upper and lower bounding surfaces, respectively, and unperturbed anchoring angle $\alpha_0^{(0)}$ at the lower bounding surface, as outlined in Secs. II C and III. The motivation for choosing these test points was that they lie nearby the most promising region of parameter space for the 1D model, but when unperturbed do not permit two-way switching [2]. Perturbing a 1D device based on these points therefore gives some insight into whether 2D effects can lead to improvements over the 1D results. The unperturbed anchoring angle at the upper bounding surface $\alpha_1^{(0)}$ is fixed by Eq. (14). Both anchoring angles are systematically perturbed according to three different protocols, described in Secs. IV A (in-phase variable-amplitude variable-wavelength perturbations to both angles), IV B (variable-phase variable-amplitude fixed-wavelength perturbations to both angles), and IV C (variable-amplitude variable-wavelength perturbations to one angle only). Where both boundaries are perturbed, the

perturbation amplitude δ is the same at each boundary; where only the lower boundary is perturbed, the phase difference ϕ is zero by default. Since only two of the three variables δ , L (domain length), and ϕ are perturbed in any set of experiments, our results on the steady states found and switching between them can be represented graphically by 2D parametric plots.

For all cases studied the perturbations lead to surprisingly rich behavior when compared with the 1D case. As we would expect, for sufficiently small δ , the results are close to those found in one dimension: only two stable steady states, with no two-way switching under transient application of an electric field. However, for a given L we find a threshold value δ^* at which a bifurcation occurs and new steady states are found. This threshold value δ^* decreases as L increases. Depending on the value of L , the new steady state(s) may either replace the continuations of the original steady states \mathbf{n}_1 and \mathbf{n}_2 [a simple pitchfork bifurcation; see Figs. 6(a), 8(a), and 11(a)] or else coexist with them [a saddle-node bifurcation; see Figs. 6(b), 8(b), and 11(b)]. Though a full bifurcation study was not performed, our results indicate that short domains (small L) lead to a pitchfork bifurcation in which bistability yields to monostability, while long domains give a more complex bifurcation structure with folds, in which multiple distinct steady states can coexist (in the cases we considered, up to four states were found simultaneously). The bifurcation to tri- and tetrastability can occur at very small δ^* for the largest L considered. Somewhat surprisingly, introducing a phase difference between perturbations at the two boundaries does not have a significant effect on the results obtained, at least for the domains considered.

On the one hand, our results indicate that long-wavelength perturbations of even very small amplitude may introduce significant complexity, in particular multiple stable steady states, but with a lack of reversible switching between them. While interesting from a scientific point of view, this finding also has a practical consequence since it suggests that such perturbations are not useful if a reliable bistable device with two-way switching is desired. This finding also suggests that an unperturbed device, of the kind discussed in Ref. [2], may be unstable if the domain length is large, with possible multistability and undesired complexity.

On the other hand, we do find a sizable set of boundary perturbations for which two-way switching is found between states \mathbf{n}_1 and \mathbf{n}_2 , for parameters for which two-way switching is not possible in the unperturbed case. Even more interestingly we find that two-way switching between the newly found \mathbf{n}_3 state and the \mathbf{n}_2 state, as well as cyclic switching $\mathbf{n}_1 \rightarrow \mathbf{n}_3 \rightarrow \mathbf{n}_2 \rightarrow \mathbf{n}_1$, may occur. Therefore, we find significant potential utility of the boundary perturbations, particularly of shorter wavelengths, provided one can make boundary modifications of wavelength comparable to or smaller than the device thickness and of reasonable amplitude. Presumably the finite-size amplitude of such perturbations would be sufficient to destroy the undesired sensitivity to long-wavelength small-amplitude perturbations noted above. Though both directions of the electric field are considered when testing for switching ($\mathcal{F} = \pm 5$), the switching is always found for $\mathcal{F} = -5$ (this was also the case for the 1D problem [2]).

We note that our results are also of interest when compared to theoretical simulations of the so-called ZBD [3]. In that

device a 2D model is found to permit bistability and two-way switching via boundary perturbations (geometric, for the ZBD); but one of the two steady states always has a disclination. Our model suggests that a truly 2D bistable switchable device may in fact be possible without any disclinations.

Throughout this study, in our switching investigations it was assumed that the electric field, when applied, is uniform throughout the NLC. In reality of course there is interaction between the field and the NLC, leading to nonuniformities in the field. A preliminary investigation into the size of such deviations from uniformity for the 1D model suggests that, under typical operating conditions, they are small [4]. We have not explored extensively the influence of the strength or duration of the applied electric field, but based on our previous analysis of the one-dimensional configuration in Ref. [2], we would not expect to see significant influence of these quantities on the presented results. (The field is simply the means by which switching is effected: As long as it is sufficiently strong and applied for sufficiently long, which we believe is the case in the present paper, then if switching is theoretically possible it should be observed.)

We do not, in this paper, carry out a detailed study of optical contrast between the stable states found since we are far from producing any kind of optimal device of this kind. We note, however, that optical contrast ratios were calculated for the 1D solutions of [2] from which our 2D solutions derive and were found to be generally good. In addition, the bifurcation plots in the present paper, showing the norm of the director field versus perturbation amplitude, provide some crude estimate of the contrast between the steady states.

In this work we have considered a three-dimensional parameter space defined by $(\mathcal{A}_0, \mathcal{A}_1, \alpha_0^{(0)})$. It is clearly difficult to analyze this large space in detail by the present methods and we certainly cannot claim that the results found at the considered isolated points cover the whole range of possible behavior. For example, we found that up to four steady states can coexist in some cases; however, even more complex scenarios with a larger number of stable solutions are possible. Despite the

limitations of the presented analysis, our results do suggest that improvements from the unperturbed 1D configurations are possible; however, the extent of these improvements may depend on the choice of physical parameters (anchoring strengths and angles). In addition, our results strongly suggest that short-wavelength perturbations are more promising if formulation of a bistable switchable device is desired. A more detailed study, beyond the scope of the present paper, is required to determine the true utility of such a device. More points in parameter space should be considered to confirm the generality of our findings for the few points studied here; for the most promising short-wavelength boundary perturbations, a detailed study of the energy landscape should be made (the energy barriers between stable states should be neither too high to surmount nor too low for robustness to shocks) and the optical contrast ratios calculated.

Finally, we note that, of course, all of our results here are restricted to two space dimensions and take no account of three-dimensional effects. The 2D problem for the director field in an NLC is rather special since \mathbf{n} may be described in terms of a single polar angle θ . If 3D variations are permitted to either device boundary then a second (azimuthal) angle φ is required to characterize the director and a system of coupled partial differential equations for θ and φ (arising from the gradient flow model due to the more complicated free energy describing 3D elastic deformation) must be solved. Even for simple classes of 3D perturbations to the bounding surfaces and for the simplest case of conical anchoring on φ at both surfaces, we might expect the results to be correspondingly richer still than those presented here.

ACKNOWLEDGMENTS

This work was supported by the NSF under Grants No. DMS-0908158 and No. DMS-1211713. L. J. C. also gratefully acknowledges partial support from King Abdullah University of Science and Technology in the form of an OCCAM Visiting Fellowship, funded by Award No. KUK-C1-013-04.

-
- [1] T. Z. Kosc, *Opt. Photonics News* **16**, 18 (2005).
 - [2] L. J. Cummings, C. Cai, and L. Kondic, *J. Eng. Math.* **80**, 21 (2013).
 - [3] G. P. Bryan-Brown, C. V. Brown, and J. C. Jones, US Patent No. 6,249,332 (19 June 2001).
 - [4] C. Cai, Ph.D. thesis, New Jersey Institute of Technology, 2013.
 - [5] T. J. Chen and K. L. Chu, *Appl. Phys. Lett.* **92**, 091102 (2008).
 - [6] L. Cui, W. Jin, Y. Liu, P. Xie, R. Zhang, C. Zhu, and C. Wang, *Mol. Cryst. Liq. Cryst.* **333**, 135 (1999).
 - [7] J. Y. Hwang, S. H. Lee, S. K. Paek, and D. S. Deo, *Jpn. J. Appl. Phys.* **42**, 1713 (2003).
 - [8] K. H. Kim, J. I. Baek, B. H. Cheong, H. Y. Choi, S. T. Shin, J. C. Kim, and T. H. Yoon, *Appl. Phys. Lett.* **96**, 213507 (2010).
 - [9] L. Komitov, G. Barbero, I. Dahl, B. Helgee, and N. Olsson, *Liq. Cryst.* **36**, 747 (2009).
 - [10] H. J. Lee, D. Kang, C. M. Clark, and C. Rosenblatt, *J. Appl. Phys.* **105**, 023508 (2009).
 - [11] C. J. Lin, G. T. Hong, and R. P. Pan, *Mol. Cryst. Liq. Cryst.* **512**, 911937 (2009).
 - [12] Y. Reznikov, R. G. Petschek, and C. Rosenblatt, *Appl. Phys. Lett.* **68**, 2201 (1996).
 - [13] D. S. Seo, *J. Appl. Phys.* **86**, 3594 (1999).
 - [14] D. S. Seo, *J. Korean Phys. Soc.* **36**, 29 (2000).
 - [15] K. E. Vaughn, M. Sousa, D. Kang, and C. Rosenblatt, *Appl. Phys. Lett.* **90**, 194102 (2007).
 - [16] W. Y. Wu, C. C. Wang, and A. Y. G. Fuh, *Opt. Express* **16**, 17131 (2008).
 - [17] F. S. Y. Yeung, F. C. Xie, J. T. K. Wan, F. K. Lee, O. C. K. Tsui, P. Sheng, and H. S. Kwok, *J. Appl. Phys.* **99**, 124506 (2006).
 - [18] E. Willman, F. A. Fernandez, R. James, and S. E. Day, *J. Disp. Technol.* **4**, 276 (2008).
 - [19] I. W. Stewart, *The Static and Dynamic Continuum Theory of Liquid Crystals* (Taylor & Francis, London, 2004).

- [20] P. G. de Gennes and J. Prost, *The Physics of Liquid Crystals*, 2nd ed., International Series of Monographs on Physics Vol. 83 (Oxford Science, Oxford, 1993).
- [21] S. Chandrasekhar, *Liquid Crystals*, 2nd ed. (Cambridge University Press, Cambridge, 1992).
- [22] L. M. Blinov, M. Kolovsky, T. Nagata, M. Ozaki, and K. Yoshino, *Jpn. J. Appl. Phys.* **38**, L1042 (1999).
- [23] P. R. M. Murthy, V. A. Raghunathan, and N. V. Madhusudana, *Liq. Cryst.* **14**, 483 (1993).
- [24] A. J. Davidson and N. J. Mottram, *Phys. Rev. E* **65**, 051710 (2002).
- [25] A. Rapini and M. Papoular, *J. Phys. (Paris) Colloq.* **30**, C4-54 (1969).
- [26] F. M. Leslie, *Adv. Liq. Cryst.* **4**, 1 (1979).
- [27] P. J. Kedney and F. M. Leslie, *Liq. Cryst.* **24**, 613 (1998).
- [28] L. J. Cummings and G. Richardson, *Eur. J. Appl. Math.* **17**, 435 (2006).